Journal of Chromatography A, 1218 (2011) 1170–1184

Contents lists available at ScienceDirect

Journal of Chromatography A

journal homepage: www.elsevier.com/locate/chroma

Kinetic performance limits of constant pressure versus constant flow rate gradient elution separations. Part II: Experimental

M. Verstraeten [a], K. Broeckhoven [a], M. Dittmann [b], K. Choikhet [b], K. Witt [b], G. Desmet [a,*]

[a] Vrije Universiteit Brussel, Department of Chemical Engineering (CHIS-IR), Pleinlaan 2, 1050 Brussels, Belgium
[b] Agilent Technologies Germany GmbH, Hewlett-Packard Str. 8, Waldbronn, BW 76337, Germany

ARTICLE INFO

Article history:
Received 1 October 2010
Received in revised form
16 December 2010
Accepted 19 December 2010
Available online 28 December 2010

Keywords:
Constant pressure
Kinetic performance
Peak capacity
Gradient plate height
Ultra-high pressure
Kinetic plot

ABSTRACT

We report on a first series of experiments comparing the selectivity and the kinetic performance of constant flow rate and constant pressure mode gradient elution separations. Both water–methanol and water–acetonitrile mobile phase mixtures have been considered, as well as different samples and gradient programs. Instrument pressures up to 1200 bar have been used. Neglecting some small possible deviations caused by viscous heating effects, the experiments could confirm the theoretical expectation that both operation modes should lead to identical separation selectivities provided the same mobile phase gradient program is run in reduced volumetric coordinates. Also in agreement with the theoretical expectations, the cP-mode led to a gain in analysis time amounting up to some 17% for linear gradients running from 5 to 95% of organic modifier at ultra-high pressures. Gains of over 25% were obtained for segmented gradients, at least when the flat portions of the gradient program were situated in regions where the gradient composition was the least viscous. Detailed plate height measurements showed that the single difference between the constant flow rate and the constant pressure mode is a (small) difference in efficiency caused by the difference in average flow rate, in turn leading to a different intrinsic band broadening. Separating a phenone sample with a 20–95% water–acetonitrile gradient, the cP-mode leads to gradient plate heights that are some 20–40% smaller than in the cF-mode in the B-term dominated regime, while they are some 5–10% larger in the C-term dominated regime. Considering a separation with sub 2-μm particles on a 350 mm long coupled column, switching to the constant pressure mode allowed to finish the run in 29 instead of in 35 min, while also a larger peak capacity is obtained (going from 334 in the cF-mode to 339 in the cP-mode) and the mutual selectivity between the different peaks is fully retained.

1. Introduction

In part I, the potential kinetic advantages of running gradient separations in the constant pressure mode instead of in the customary constant flow rate mode have been theoretically assessed. The direct motivation for this work was the desire to maximally exploit the kinetic advantages of maximum pressure separations. This maximal pressure can be the nominal pressure limit given by the column or pump manufacturer, but can also lie at a lower value, specified by the user to prolong the column lifetime or to limit the pump failure risks.

During a gradient elution separation conducted in the constant flow rate mode (cF-mode), the maximum pressure is usually only reached during a brief instant, namely at the moment at which the mobile phase running through the column reaches its viscosity maximum. In the constant pressure mode (cP-mode) on the other hand, the pump is kept at the maximal pressure and will thus deliver a larger flow rate during most of the gradient run. As a consequence, the elution of the sample components is sped up and the run time is shortened.

In a sense, the cP-mode operation bears some resemblance to the so-called flow programming technique that attracted some attention in the early days of HPLC as a possibility to speed up the elution of the late eluting compounds in isocratic runs [1–5]. This technique has, however, never gained much popularity because of the much more powerful possibilities of mobile phase gradient elution [1] and only a limited number of applications has been reported [6–8]. Despite the apparent resemblance, the cP-operation fundamentally differs from the flow programming technique because of the applied pressure profile. In flow programming, the pressure is gradually increased during the course of the separation. As a consequence, the flow programming technique only makes a sub-optimal use of the available pressure during most of the separation run, whereas it is precisely the aim of the cP-mode operation to oper-

* Corresponding author. Tel.: +32 02 629 32 51; fax: +32 02 629 32 48.
E-mail address: gedesmet@vub.ac.be (G. Desmet).

0021-9673/$ – see front matter © 2010 Elsevier B.V. All rights reserved.
doi:10.1016/j.chroma.2010.12.087

ate at the kinetic optimum conditions (i.e., at maximal pressure) during the entire separation.

Attempts to combine the advantages of both flow programming and gradient elution have been proposed, amongst others, by Lesins and Ruckenstein [9] and Nikitas and Pappa-Louisi [10–12]. These authors, however, did not consider the case wherein the flow program and the gradient elution program are coupled by the mobile phase viscosity, as is the case in the cP-gradient elution. A classic example of a cP-operation is of course to be found in the field of GC, where most instruments were originally operated in the constant pressure mode. Nowadays, most GC instruments are, however, operated in the constant mass flow rate mode [13,14]. cP-systems were certainly also quite common in the early days of LC. A more recent example (1997) is the work of Chen and Horvath who have used a cP-system to investigate the combined effect of mobile phase and temperature gradients [15]. A more complete review on the literature on gradient elution and flow programming is given in part I.

In part I, it has been shown that, despite its varying flow rate, and shorter run time, a cP-gradient separation can offer the same selectivity as that obtained in the cF-mode (except from some small differences induced by the difference in pressure and viscous heating history, see part I), provided both systems are run with the same volume-based gradient program, i.e., with a gradient program that is programmed as a function of the pumped volume instead of a function of the elapsed time.

The volumetric units are also needed to correctly quantify the separation selectivity (determined by the effective retention coefficient k_{eff}) and the separation efficiency (determined by σ_V or H). The customary used time-based chromatogram indeed no longer correctly represents the separation state in the column when the flow rate varies with the time, whereas the volume-based chromatogram still does.

However, for those reluctant to use volumetric units to plot chromatograms and/or program gradients, the volume scale coordinate can be directly transformed into a reconstructed time t_V, simply obtained by dividing the volume data by an arbitrary constant flow rate value F, e.g. by the flow rate of the corresponding cF-run F_F (being the minimal flow rate during the cP-run) to allow direct comparison of results:

$$t_v = \frac{V}{F_F} \tag{1}$$

Because of the linearity of this rescaling, cP-mode chromatograms that are plotted vs. the reconstructed time display exactly the same relative elution pattern as when plotted versus the volume. Programming a gradient in volumetric units instead of in time units is also straightforward, as it can be based on the same type of rescaling as that leading to the reconstructed time (cf. Eq. (1)). This was illustrated in Table 1 of part I for the case of a relatively complex gradient pattern. For linear gradient programs, the translation between time- and volume-based coordinates is even more straightforward, because the condition of a constant flow rate in the cF-mode automatically implies that the ratio of t_G/t_0 in the time-based program is equal to the ratio of V_G/V_0 (wherein V_G is the total gradient volume). As a consequence, the gradient steepness factor is identical in either time units or in volumetric units in the cF-mode:

$$\beta t_0 = (\phi_e - \phi_0) \cdot \frac{t_0}{t_G} = (\phi_e - \phi_0) \cdot \frac{V_0}{V_G} = \beta V_0 \tag{2}$$

With this definition, the expressions for the effective retention coefficient k_{eff} and for the retention coefficient at the moment of elution $k_{loc,e}$ that are obtained for a linear volume-based gradient (see Refs. [16–20] and also part I) are fully similar to the well-established expressions obtained for time-based gradients [21–24]:

$$k_{eff} = \frac{\ln(k_0 S\beta V_0 + 1)}{S\beta V_0} \tag{3}$$

$$k_{loc,e} = \frac{k_0}{k_0 S\beta V_0 + 1} \tag{4}$$

The only difference with the time-based variant is that t_0 is now replaced by V_0 (note that that $S\beta V_0$ is equal to Snyder's b-parameter [18] and Neue's G-parameter [23,25]). Whereas the time-based variant is only valid in the cF-mode, Eqs. (3) and (4) hold for the cF- as well as the cP-mode. In fact, they hold for any possible variable flow rate trajectory.

Recalling from part I that the retention factor can only be correctly determined in a volume-based chromatogram, or in its linearly rescaled reconstructed time-based chromatogram, it should be noted that the effective retention coefficient k_{eff} appearing in (3) should be defined as:

$$k_{eff} = \frac{V_R - V_0}{V_0} = \frac{t_{V,R} - t_{V,0}}{t_{V,0}} \tag{5}$$

where V_R is the run volume at the moment of elution and $t_{V,R}$ is the corresponding elution time in reconstructed time units, calculated by using $V = V_R$ in Eq. (1).

In the present part, it is investigated to which extent the theoretical findings discussed in part I can be implemented in practice. This implementation first of all requires the availability of run volume data at any time (e.g. total mobile phase volume delivered since the start of the analysis run), and the ability of the instrument to generate in real-time a mobile phase composition gradient as a function of the delivered volume rather than of elapsed time. For this purpose, dedicated prototype firmware has been designed and installed on the instrument. Using this set-up, measurements have been conducted to validate the theoretical gain in analysis time in the cP-mode that was theoretically calculated in part I, as well as to experimentally observe the similarities and differences in selectivity and (kinetic) performance when comparing the cP- to the cF-elution mode. Since the potential gains in analysis time and/or peak capacity that have been forecasted in part I were obtained under the assumption that the effects of ultra-high pressures and the concomitant viscous heating on the difference between the cP- and the cF-operation can to a first approximation be neglected, the quality of this assumption certainly needs to be verified experimentally. For this purpose, experiments have been conducted at pressures up to 1200 bar.

2. Experimental

2.1. Chemicals and columns

An RRLC checkout sample (mixture of phenones) was provided by Agilent Technologies (Waldbronn, Germany). Uracil, thiourea, benzene, toluene, ethylbenzene, propylbenzene, mesitylene and pyrene were purchased from Sigma–Aldrich (Steinheim, Germany). Acetonitrile (ACN) and methanol (MeOH) were also purchased from Sigma–Aldrich, HPLC grade water (H_2O) was prepared in the laboratory using a Milli-Q gradient (Millipore, Bedford, MA, USA) water purification system. The alkylbenzene mixture consisting of 0.04 mg/mL uracil, 2.3 mg/mL benzene, 2.3 mg/mL toluene, 2.4 mg/mL elthylbenzene, 2.4 mg/mL propylbenzene, 2.4 mg/mL mesitylene and 0.22 mg/mL pyrene was dissolved in 66/33% MeOH/H_2O. The phenone mixture (sample lot no. CG-0609) consisting of acetophenone, propiophenone, butyrophenone, valerophenone, hexanophenone, heptanophenone, octanophenone, benzophenone and acetanilide, each in a concentration of 0.10 mg/mL, and 0.15 mg/mL thiourea was

dissolved in 43/57% ACN/H_2O. Zorbax Eclipse Plus RRHD C_{18} columns (150 mm × 2.1 mm, 1.8 μm; 100 mm × 2.1 mm, 1.8 μm) were provided by Agilent Technologies (Waldbronn, Germany). The performance of the individual columns was measured by an injection of 0.08 mg/mL naphthalene (HPLC-grade) in a 60 vol% ACN mobile phase ($k'_{ave} = 4.3$). The number of theoretical plates was 35,216, 21,845 and 22,426 for the 150 and two 100 mm columns, respectively.

2.2. Apparatus and methodology

The experiments were conducted on an Agilent 1290 Infinity system with a binary pump that can deliver a flow rate of 2 mL/min at 1200 bar. The system's maximum flow rate increases linearly with decreasing operating pressure to a maximum of 5 mL/min at 800 bar. The pumped mobile phase was mixed with a Jet Weaver mixer with a volume of 35 μL. The system also consisted of a variable wavelength detector with a low dispersion cell (2 μL volume and 3 mm path length), an autosampler and a thermostatted column compartment with a 1.6 μL mobile phase preheater. The system was operated with Agilent Chemstation software with an adapted firmware that has been designed to allow the pump to run gradient programs vs. run volume (actually delivered volume since run start) and to provide a real-time output for the run volume over time. The firmware of the pump keeps track of the run volume (pumped volume) and adjusts the pumped mobile phase composition according to the gradient program in a way that the composition vs. run volume trace is maintained the same, independent of possible flow rate variations.

For the cP-experiments, all methods were set to the same pressure as the maximum pressure observed during the cF-runs. While the viscosity change in the course of the gradient resulted in non-constant flow rate, the gradient slope in volumetric units (V_G/V_0) was kept the same in cP- and cF-mode as a result of operating gradient programs vs. run volume.

The data for both run modes were acquired vs. real time and later converted to be displayed vs. reconstructed time or run volume using the run volume vs. real time dependency data, supplied by the firmware routines of the pump. Based on these data, other signals (e.g. absorbance vs. time) were also transferred to the volume domain and further processed as function of volume.

All experiments were conducted in the gradient mode. For the measurements with the alkylbenzene mixture, gradients were run from an initial mobile phase of 50/50 (%, v/v) MeOH/H_2O to 100/0 (%, v/v) MeOH/H_2O at a gradient steepness V_G/V_0 of 9.25. For the measurements with the phenone mixture, the initial mobile phase was 20/80 (%, v/v) ACN/H_2O, the final mobile phase 95/5 (%, v/v) ACN/H_2O and the gradient steepness V_G/V_0 was 12.24. A more complex gradient program consisting of three segments (linear, isocratic and linear gradient) was executed as well. Both the alkylbenzene and phenone mixture were measured on a 150 mm column. Supplementary, the alkylbenzene mixture was measured on a coupled 250 mm column at the maximal pressure and the phenone mixture was measured on a coupled 250 mm and 350 mm column. For these measurements, the gradient volume V_G was increased in proportion to the increase in total column volume V_0 to ensure that the same gradient program was run in relative volumetric units. Also an additional delay volume V_{dwell} was added before the start of the gradient to ensure that the ratio of delay volume to V_0 was kept constant. The system dwell volume was determined using the procedure described in [26] and was determined as 112 μL.

For every component in the chromatogram, the peak widths were determined at half height. All experiments were conducted at a temperature of 30 °C. The injected sample mixture volume was 0.5 μL. Absorbance values of the alkylbenzene and the phenone mixture were measured at 254 and 245 nm, respectively, with a sample rate of 80 Hz. The efficiency measurements were conducted from the lowest flow rate (0.025 mL/min) up to the maximal available pressure of the instrument (1200 bar).

3. Results and discussion

3.1. Evolution of pressure, flow rate and pumped volume in the cP-mode and cF-mode

Fig. 1a shows an example of the *P*- and *F*-trace as recorded on the instrument in the cP-mode (black curves) and the cF-mode (red curves). In both modes, the same 5–95% water–methanol volume-based gradient program was run until its end composition has reached the end of the column. Considering first the cF-mode, it is obvious to see that the corresponding *F*-trace runs perfectly flat. The inlet pressure *P* on the other hand varies strongly with the time, as a consequence of the fact that the column-averaged viscosity $\bar{\eta}$ varies with the time in a gradient run. The corresponding pressure variation is dictated by Darcy's law:

$$\Delta P_{col} = \frac{F\bar{\eta}L}{A\varepsilon_T K_{V_0}} \quad (6)$$

Since all other parameters are constant, Eq. (6) readily shows that the measured pressure trace is in fact a direct measure for the variation in column-averaged viscosity $\bar{\eta}$ in the cF-mode ($\Delta P_{col} \sim \bar{\eta}$). Note that Darcy's law cannot be based on a local value for the viscosity because the viscosity gradually varies in the column not only depending primarily on local mobile phase composition but also on local pressure and temperature.

In the cP-mode (black curves), the roles of pressure and flow rate in Eq. (6) are switched, so that in this case the pressure stays constant while the flow rate varies inversely proportional to the varying column-averaged viscosity $\bar{\eta}$ ($F \sim 1/\bar{\eta}$). Fig. 1a also shows that the flow rate in the cP-mode is always higher than or equal to that in the cF-mode, as a consequence of the higher operation pressure in the former. The average increase in flow rate that can be calculated on the basis of the two flow rate curves is about 19%, a value lying slightly above the theoretically expected value of 17.7% that can be read out from Table 3 of part I for a 5–95%-gradient with $V_G/V_0 = 15$ ($V_G/V_0 = 16$ in the present experiment).

The fact that the traces for the cP-mode stop at an earlier point in time than in the cF-mode is obviously a direct consequence of the higher average flow rate in the cP-mode and of the employed time-based representation, combined with the fact that in both cases the same volume-based gradient has been followed, i.e., the same gradient volume has been pumped. If the traces would have been plotted versus the run volume *V*, the cF- and cP-mode curves would have stopped at the same point.

If the data would have been plotted versus the run volume (data not shown), the curves for *F* (cP-mode) and P (cF-mode) would also have run in an exactly inversely proportional relation, because the column-averaged viscosity $\bar{\eta}$ follows in both modes the same relation to *V* (because the same volumetric gradient program is produced by the modified firmware in the pump). According to Eq. (6), it indeed automatically follows that:

$$F_{P\text{-mode}} \div \frac{1}{P_{F\text{-mode}}} \quad (7)$$

Fully similar observations as those discussed above were made for a 5–95% water–acetonitrile gradient (data not represented here). The only difference is the actual trajectory followed by the *F*- and *P*-traces, as a direct consequence of the fact that water–methanol mixtures display a different relation between η and ϕ than water and acetonitrile mixtures. This difference is illustrated in Fig. 1b, comparing the *P*-trace in the cF-mode for the

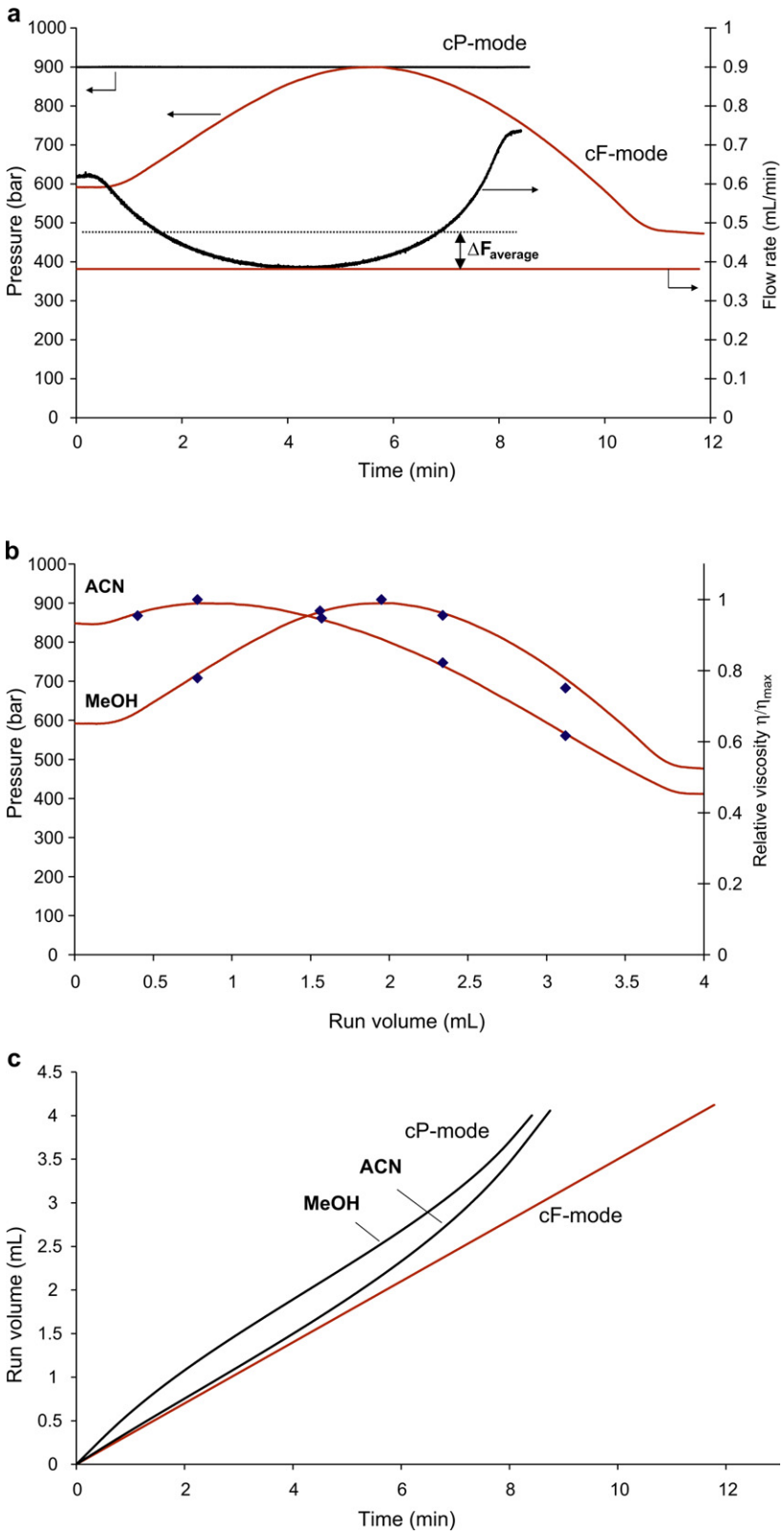

Fig. 1. (a) Pressure and flow rate trace for elution in the cP-mode (black) and the cF-mode (red) for a linear water–methanol gradient (ϕ_0 = 5%, ϕ_e = 95%) at a pressure of P_{max} = 900 bar, corresponding to F_{min} = 0.38 mL/min. (b) Pressure trace for a linear water–methanol and water–acetonitrile gradient versus run volume (ϕ_0 = 5%, ϕ_e = 95%) at a flow rate such that P_{max} = 900 bar. The solid data points represent the relative viscosity data (fitted to the maximum of the pressure curve) for water–methanol and water–acetonitrile mixtures obtained from independent experimental measurements [27]. (c) Run volume versus time for a linear water–acetonitrile and water–methanol gradient in the cP-mode (black) and the cF-mode (red). All measurements were performed on a 2.1 mm × 100 mm column. (For interpretation of the references to color in text, the reader is referred to the web version of the article.)

case of a water–acetonitrile and a water–methanol gradient. Since the two curves in Fig. 1b relate to a linear volume-based gradient program (so that ϕ varies linearly with the V-coordinate) and since $\Delta P \sim \bar{\eta}$ (cf. Eq. 6), the curves of P versus V in Fig. 1b are directly proportional to the relation between the column-averaged viscosity and the column-averaged fraction of organic modifier ϕ ($\bar{\eta}$ versus ϕ). As a consequence, the P-traces shown in Fig. 1b can be expected to follow a trajectory that is quasi-identical to the well-established η versus ϕ curves reported in literature. To verify this, the relative viscosity data for water–methanol and water–acetonitrile mixtures obtained from independent experimental measurements [27] have been added to Fig. 1b. These data correspond to those shown in Fig. S-1 of the SM of part I and also agree very well to other literature sources providing physicochemical data for water–organic modifier mixtures [28,29]. The good agreement shows that the difference between $\bar{\eta}$ (the column-averaged viscosity) and η_{peak} (the point-wise value of viscosity) mentioned in the discussion leading up to Fig. 4c of part I is very small, at least in the range of $V_G/V_0 > 10$, which is anyhow the range wherein most gradients are executed [30]. The flat parts at the end and the beginning of each of the recorded P-curves are due to the fact that the mobile phase composition in the column does not vary linearly with the pumped volume at the beginning and the end of the gradient but tends to become constant (i.e., before the start of the gradient slope breaks through at the end of column and after the end of the gradient slope has passed the column inlet). Other than this, the recorded P-traces display an excellent agreement with the thermodynamic data on the relation between the viscosity and the mobile phase composition. The water–methanol curve for example displays the well-known features of the (η, ϕ)-relationship of water–methanol mixtures [27–29]: starting from a relatively low value at $\phi = 5\%$ (about 65% of the viscosity maximum) in the beginning of the gradient, the viscosity first increases steadily with ϕ, then goes through a maximum around $\phi = 50\%$ and then decreases again with somewhat steeper slope towards the $\phi = 95\%$ point (where the viscosity is about 53% of the viscosity maximum). Also in agreement with [27–29], the water–acetonitrile curve is also in perfect agreement with the (η, ϕ)-relationships that can be found in literature, displaying only a very slow increase of the viscosity with ϕ for small ϕ and reaching its maximum around $\phi = 20\%$. After this maximum, the viscosity drops rather steeply.

Because of this varying viscosity, and the correspondingly varying flow rate, the cP-mode operation leads to a complex relation between the pumped volume and the time, as is shown in Fig. 1c (cf. the black curves). The difference between the methanol and the acetonitrile is purely due to the difference in their viscosity profile, since the slope of the run volume vs. time curve equals to the flow rate which is inversely proportional to the column-averaged viscosity in the cP-mode. In the cF-mode, where the flow rate is meant to be constant, the relation between the volume and the time obviously needs to be perfectly linear. As can be noted from the red line in Fig. 1c, this is indeed the case.

3.2. Difference and equivalence of chromatograms recorded in the cP-mode and cF-mode

Fig. 2a shows an example of the real-time chromatograms obtained with the phenone sample and a water–acetonitrile gradient in the cF- and cP-mode (the pressure in the cP-run corresponds to the maximal pressure of the cF-run) at a relatively high velocity, i.e., well above the optimal flow rate (see discussion of Fig. 7 further on). Because of the higher average flow rate, the compounds clearly elute faster in the cP-mode. Considering the elution of the last compound, the cP-mode separation finishes some 17.1% faster than the cF-mode separation. To compare this gain value with the theoretical expectations, it should first of all be noted that the gain percentage is based on the elution time of the last compound. This compound elutes when the composition at the column inlet is at $\phi = 93.9\%$, i.e., at the moment where the end of the gradient has not reached the column inlet. The theoretically expected time gain should hence be calculated using Table S-9a (case = water–acetonitrile, $V_G/V_0 = 12.24$, average column pressure = 500 bar) of the SM of part I. Interpolating between the $\phi_e = 90\%$ and the $\phi_e = 95\%$ data entries, a value of 17.7% is found, lying close to the experimentally observed value.

Switching from the cF- to the cP-mode clearly allows to maintain the selectivity of the separation very well, as can be witnessed from the fact that the cF- and the cP-separations nearly perfectly overlap when plotted in either the volume-based coordinates or in the reconstructed time coordinates (Fig. 2b). The reconstructed time is represented via the double x-axis and has been introduced in Eq. (1). As discussed in part I, the reconstructed time is identical to the real time for the cF-mode and is proportional with the volume in the cP-mode, so that the selectivity of the volume-based chromatogram is fully retained. The excellent overlap observed in Fig. 2b implies that when a cP-mode separation is plotted in reconstructed time, the peaks in the chromatogram will have the same retention times as those observed in the real time chromatogram of the cF-mode. Zooming in on the last peak of the volume-based chromatogram (see inset), it can be noted that the peak obtained in the cF-mode is slightly, yet significantly narrower than in the cP-mode. This is further discussed in Section 3.3.

Fig. 2 also shows the mobile phase gradient profile that was pumped by the instrument (% organic modifier) in overlap. The pumped mobile phase gradient profile in real time units (Fig. 2a), was recalculated to volume units by using the measured run-volume vs. time relationship (see Fig. 1c). The gradient profile that is run in the cP-mode is clearly non-linear in time, but this is not relevant since the analytes anyhow only react to the gradient they experience in volumetric units, a well-established fact since the early days of the gradient elution theory [17,19,20,31–33] (see Introduction of part I). In volumetric coordinates, the pumped mobile phase gradients in the cF- and the cP-mode perfectly overlap (see Fig. 2b), in agreement with the fact that the cF- and the cP-gradient were both programmed to be linear in volume (or reconstructed time) with the same gradient slope (see Eq. (2)).

Fig. 3 shows the corresponding chromatograms obtained for the same sample and gradient conditions as the separation shown in Fig. 2, but now at a significantly smaller flow rate, i.e., well below the optimal flow rate (see discussion of Fig. 7 further on). Again the separation selectivity is nearly perfectly maintained between both modes (cf. the overlap in Fig. 3b), while the cP-mode run finishes in a significantly shorter time. The difference in required analysis time is in this case some 24%, in good agreement with the theoretical expectation of about 23.1% that can be found in Table S-9b of the SM of part I (case = water–acetonitrile, $V_G/V_0 = 12.24$, average column pressure = 50 bar) when interpolating between the $\phi_e = 90\%$- and the $\phi_e = 95\%$-data entries to find the gain value corresponding to the $\phi = 93.8\%$-gradient composition at which the last compound was found to elute from the column.

An important remark that should be made here is that the gain in separation time at the lower velocity considered in Fig. 3 is significantly larger than that observed in Fig. 2 for the high velocity experiment (24% versus 17%). Given that in both cases a good agreement with the theoretical expectations was obtained, this difference can nearly be fully attributed to the different (η, ϕ)-relationship prevailing at different pressures, as can be noted from the viscosity data shown in Fig. S-1 of the SM of part I. The curves that are represented there show that the slopes left and right to the viscosity maximum of the (η, ϕ)-curves are indeed steeper at lower pressures [27,28]. As a consequence, the margin for a flow rate increase in the cP-mode is larger, thus explaining the larger time

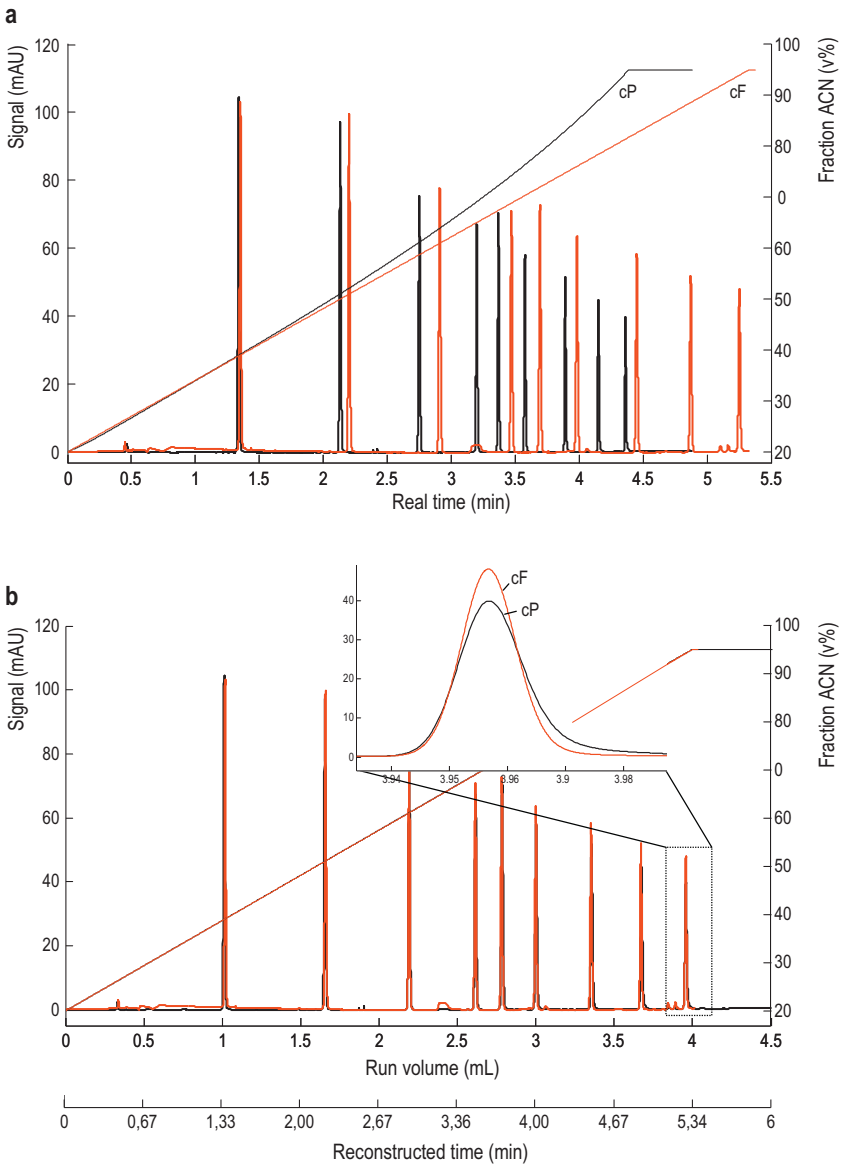

Fig. 2. Comparison of the chromatograms and the gradient program in cF- (red) and cP-mode (black) of the phenone mixture in the high velocity region (P_{max} = 1037 bar, F_{min} = 0.75 mL/min, 2.1 mm × 150 mm column) plotted versus the (a) real time and the (b) elution volume. A linear water–acetonitrile gradient was imposed: ϕ_0 = 20%, ϕ_e = 95%, V_G/V_0 = 12.24. (For interpretation of the references to color in text, the reader is referred to the web version of the article.)

gain at low pressures. Obviously this larger time gain is practically not very relevant because one would anyhow try to operate at the highest pressure. Nevertheless, the above discussion should have made clear that the time gain that can be expected for the cP-mode depends to some extent on the considered maximal operating pressure, as a consequence of the dependency of the (η, ϕ)-relationship on this pressure.

The gains realized in Figs. 2 and 3 will in practice even be larger, because in cP-mode there is no need to leave a pressure safety margin which is required in cF-mode operation. When the column permeability would reduce, e.g. as a result of column degradation, the flow rate will inevitably decrease in the cP-mode (cf. Eq. (6)), thus decreasing its gain in absolute analysis time with respect to the cF-mode. The gain will, however, still remain significant, since first only the safety margin will be progressively used up when the permeability drops further. The gains given in Tables 2–5 of part I hence remain within reach up till the point where the permeability of the column has dropped so far that the minimal flow rate in the cP-mode would be equal to that wherein the cF-mode would hit the pressure limit of the system. At this point another advantage of the cP-mode arises because in the cF-mode one has no other option than to simply replace the column, whereas the column can still be continued to be used in the cP mode, up till a point where the increase in analysis time would become unacceptable. A reduction of the column permeability during the column life time will, however, not change the retention volume of the compounds (and equivalently their 'reconstructed' retention time) since the same volume of mobile phase is always needed to elute the compounds.

Comparing the zoom-in of Fig. 3b with that in Fig. 2b, showing the detailed overlap of peak number 9, it is striking to note that the cP-peak is broader than the cF-peak in Fig. 2b (high flow rate), whereas the opposite can be observed in the zoom-in of Fig. 3b (low flow rate). These observations were consistently made and are in agreement with the numerical simulations performed in part I, as is discussed in detail further on in Section 3.3. The difference in band broadening was less pronounced for the other peaks (data not shown). This is due to the fact that, in the presently considered example, the experienced velocity difference between the cP- and

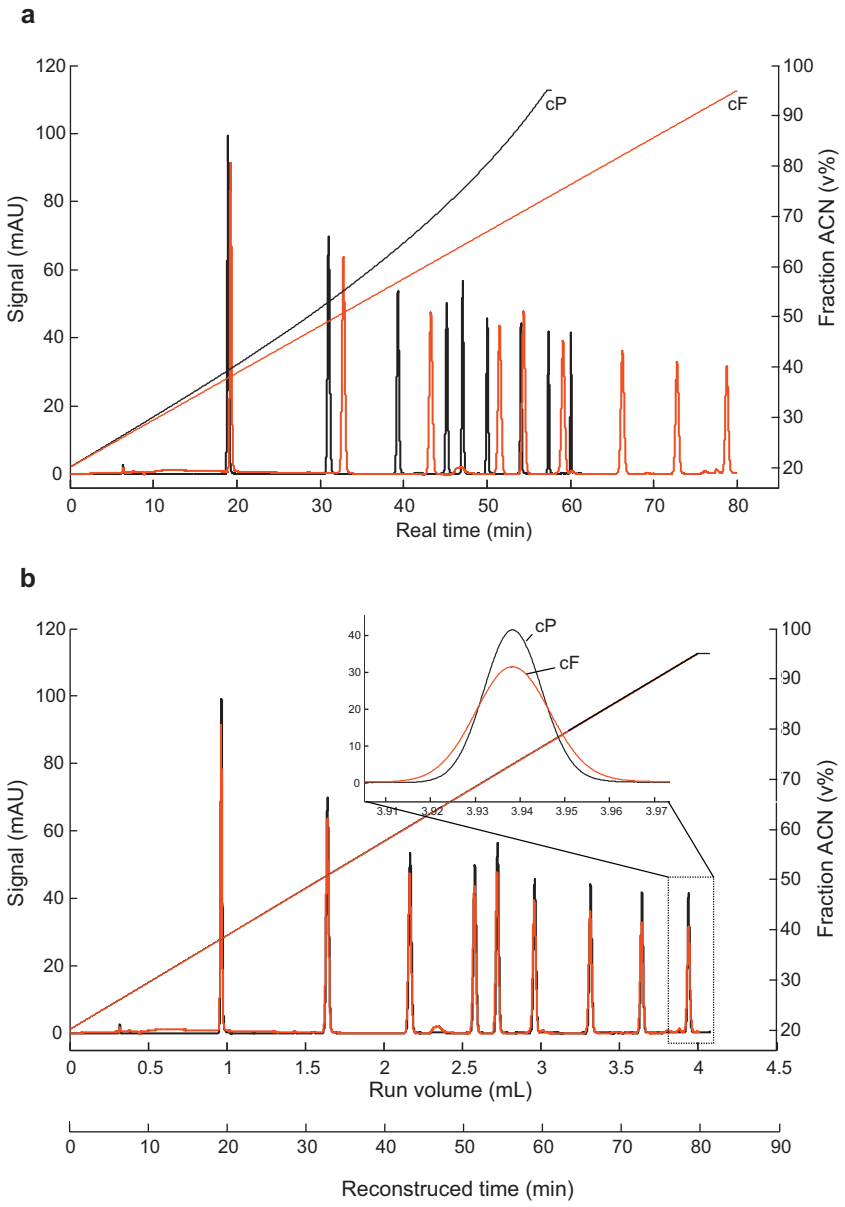

Fig. 3. Comparison of the chromatograms and the gradient program in cF- (red) and cP-mode (black) of the phenone mixture in the low velocity region (P_{max} = 88 bar, F_{min} = 0.05 mL/min, 2.1 mm × 150 mm column) plotted versus the (a) real time and the (b) elution volume. The same gradient conditions as in Fig. 2 were used. (For interpretation of the references to color in text, the reader is referred to the web version of the article.)

the cF-mode is largest for the last eluting peak. This is in turn a consequence of the fact that, in the present example, the gradient runs from the viscosity maximum (ϕ_0 = 20%) where the velocity difference is zero to a range where the viscosity is at its lowest. As a consequence, the margin for a flow rate progressively increases during the course of the gradient.

The zoom-ins shown in Figs. 2b and 3b also show that both operation modes lead to nearly equal peak areas. If used in combination with a concentration-sensitive detector such as a UV-absorption cell, the cP-mode is indeed expected to lead to the same peak area after conversion of the chromatogram to the volume or reconstructed time domain. This was confirmed by making 42 injections (at different flow rates) where was found that the relative standard deviation in peak area in the volume domain for the cP-mode was 0.45% and for the cF-mode 0.51%. The maximal difference in peak area was 2.45% and 2.14% for the cP- and cF-elution mode, respectively (all 9 compounds of the phenone mixture were considered). For the zoom-ins shown in Figs. 2b and 3b, the actual difference was measured to be about 1.5% for the peaks under consideration. On the other hand, if one would consider the real time domain, the peak area (in time) will be different in the cP-mode than in the cF-mode, being a direct consequence from the fact that the velocity during the elution of the peak under consideration is not constant.

Fig. 4 provides a more detailed study of the difference in elution behavior between the cF- and the cP-mode by plotting the effective retention factors k_{eff} (calculated in the volume-based chromatogram) for peak number 9 and number 2 for an extensive series of different flow rates. In both operating modes, the k_{eff}-values display the typical decrease already observed in other ultra-high pressure studies and which could be attributed there to the increase in mobile phase temperature originating from the viscous heating that progressively heats up the mobile phase [34,35]. The most important conclusion that can be drawn from Fig. 4 for the purpose of the present study is that the cF- and the cP-mode lead to very similar k_{eff}-values. Considering the actual elution volume (data not shown), the observed differences were even smaller

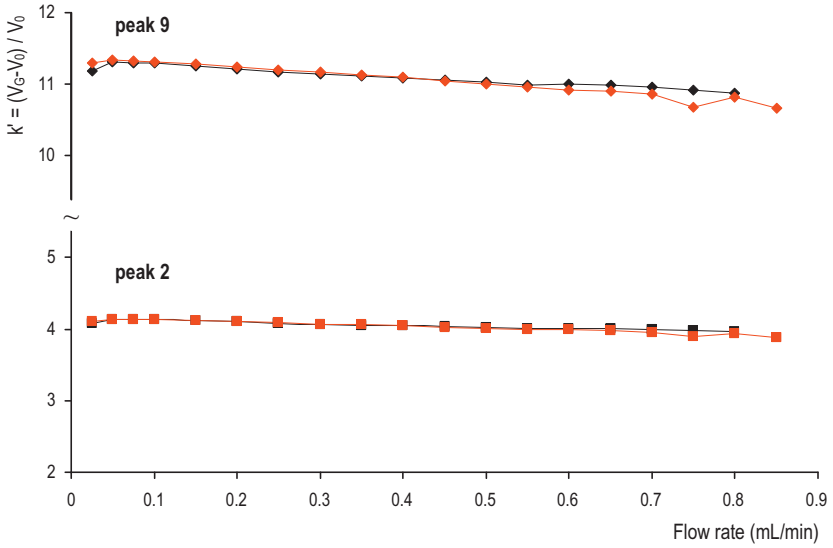

Fig. 4. Effective retention coefficients in the cF- (red) and the cP-mode (black) of peak 2 and peak 9 of the phenone mixture (same gradient conditions as in Fig. 2). The effective retention coefficient is calculated with Eq. (5). (For interpretation of the references to color in text, the reader is referred to the web version of the article.)

(average difference of some 0.3%). Considering 42 injections made at different flow rates, the relative standard deviation in retention volume was 0.39% and 0.40% for the cP- and cF-elution mode, respectively, showing a good reproducibility of retention volumes or retention times in the reconstructed time domain. In the real time domain, the relative standard deviation of 4 sequent injections was 0.30% and 0.05% for the cP- and cF-elution mode, respectively. The poorer reproducibility of the cP-measurements is attributed to the pressure controlling of the prototype firmware.

To demonstrate that the findings in Figs. 2 and 3 can be generalized, Fig. 5 shows the chromatograms of the separation of another sample (mainly alkylbenzenes) and using a water–methanol gradient instead of an water–acetonitrile gradient. Again, a significant gain in analysis time can be noted, as well as an excellent overlap in volumetric or reconstructed time coordinates. As can be noted from the real time chromatogram in Fig. 5a, the gain in analysis time amounts up to some 17.6%, again in good agreement with the 16.0% gain predicted that can be found in Table S-8 of the SM of part I (case = water–methanol, $V_G/V_0 = 9.25$, average column pressure = 500 bar) when interpolating between the $\phi_e = 95\%$- and the $\phi_e = 100\%$-data entries to find the gain value corresponding to the $\phi = 98.4\%$-gradient composition at which the last compound was found to elute from the column.

Considering that the cases considered in Figs. 1–3 and 5 lead to relative time gains that are close to the theoretically expected values, which were obtained under the assumption of a non-isothermal operation, it can be inferred that the inevitable difference in viscous heating between the cF- and the cP-mode might only have a limited effect on the observed gain (the separation in Fig. 3 relates to a low pressure separation where viscous heating is anyhow unimportant). The difference in viscous heating between the cF- and the cP-mode is inevitable because both modes inevitably have a different average operating pressure. As explained in Section 9 of part I, this effect can be expected to be relatively small, and in the advantage of the cP-mode (because the decrease in viscosity originating from the stronger viscous heating dominates the increase in viscosity originating from the higher pressure). It is anyhow difficult to draw any firm conclusion from the present study, because the observed differences occurred in both directions. Sometimes the gain was a bit larger than expected (see cases in Figs. 1 and 5 as an example), whereas sometimes the gain was smaller than expected (see case in Fig. 2 as an example). We believe this ambiguity first of all shows that the effect is small, and second, the observed time gains might also have been influenced by some pressure and flow disturbances in the initial phase of separation/gradient, attributed to limitations of the initial implementation of the prototype equipment. A future study is planned wherein the effect of viscous heating is investigated more in-depth. The potential effect of viscous heating is anyhow not easily amenable to general quantitative predictions, as the governing temperature in the column also partly depends (because of the thermal inertia) on the heating events preceding the actual separation.

To illustrate that a cP-mode and an cF-mode separation running the same volumetric gradient not only lead to the same selectivity for the case of a linear gradient, but also holds for more complex, segmented gradients is demonstrated in Fig. 6 for an water–acetonitrile gradient consisting of 2 linear segments (with different slopes) separated by an isocratic segment (phenone sample). In this particular case, the gain in analysis time even amounts up to 27%, i.e., significantly higher than can be expected for linear gradients, at least when considering typical UHPLC-pressures. The fact that a larger gain is obtained than in the linear gradient cases considered in Figs. 2 and 3 can be explained by the fact that the flat portions of the gradient in the represented example are situated in a ϕ-range where the viscosity is small, so that the cP-mode can benefit maximally from its increased flow rate during a relatively long time. Of course, the gain will be smaller than in the linear gradient for the opposite case, i.e., when the flattest portions of the gradient program are mainly situated close to the viscosity maximum, where the margin for a flow rate increase is only very small.

3.3. Fundamental band broadening measurements

As discussed in part I, it can be expected that the cP-mode and cF-mode will lead to a slightly different efficiency or band broadening when the flow rate is significantly larger or smaller than the optimal flow rate. To investigate this experimentally, the separations shown in Figs. 2 and 3 were repeated for a wide range of flow rates on a column with given length (each velocity was run in triplicate). For each velocity, the band broadening of each peak was characterized by its volumetric variance σ_V^2, which was subsequently corrected by the $(1 + k_{loc,e})$-factor to yield the true, column-averaged separation

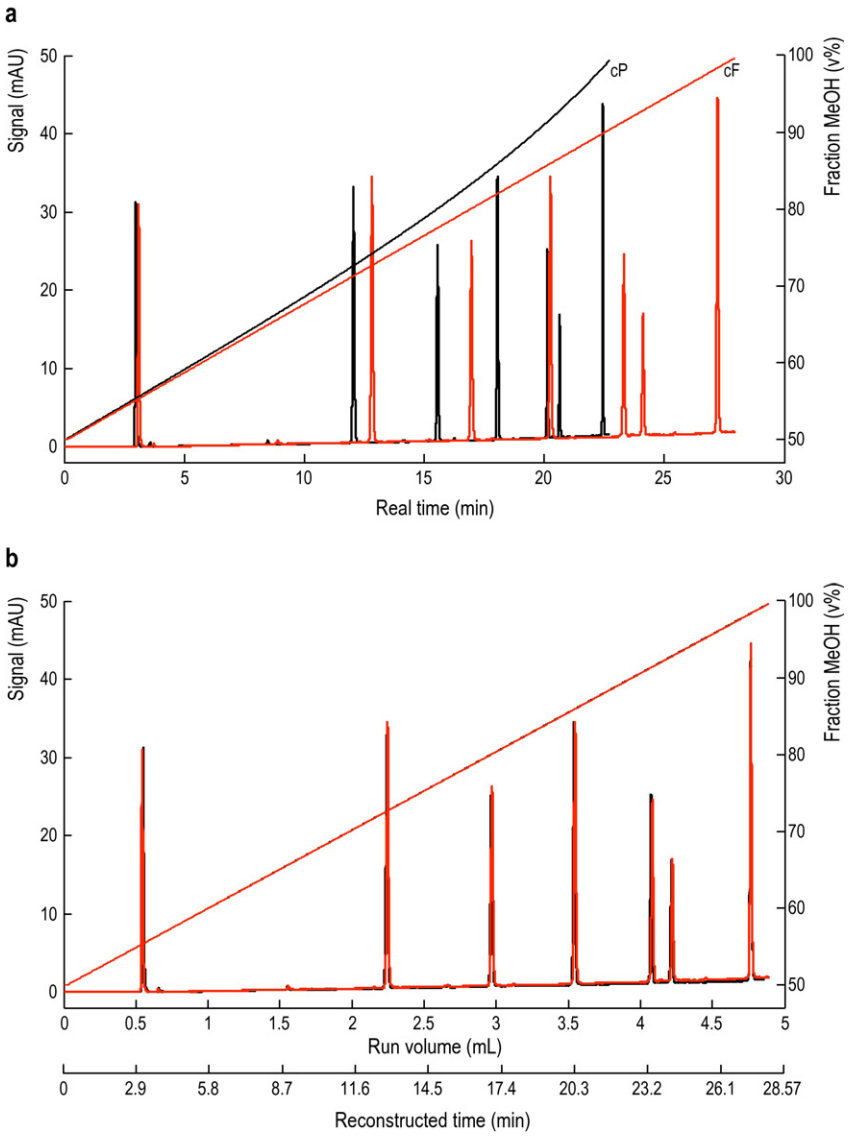

Fig. 5. Comparison of the chromatograms and the gradient program in cF- (red) and cP-mode (black) of the alkylbenzene mixture plotted versus the (a) real time and the (b) elution volume. The chromatograms were measured on a coupled 25 cm column (P_{max} = 1030 bar, F_{min} = 0.175 mL/min, 2.1 mm × 250 mm column). A linear water–methanol gradient was imposed: ϕ_0 = 50%, ϕ_e = 100%, V_G/V_0 = 9.25. (For interpretation of the references to color in text, the reader is referred to the web version of the article.)

efficiency N [25] and the column-averaged plate height H_{eff}, using:

$$H_{eff} = \frac{L}{N} = \frac{\sigma_V^2}{V^2} \cdot \frac{1}{(1 + k_{loc,e})^2} \cdot L \quad (8)$$

The retention coefficient at elution $k_{loc,e}$ was determined by running six gradients with different slopes (V_G/V_0 = 15, 20, 25, 50, 75 and 100, ϕ_0 = 20% and ϕ_e = 95%) for one of the considered flow rates (0.7 mL/min). For every peak in the chromatogram, a set of six equations was obtained (Eq. (3) for every gradient slope) and the solvent strength parameter S and k_0 were calculated by a least square fitting of the two unknowns. Consequently, the retention coefficient at elution $k_{loc,e}$ was calculated with Eq. (4).

Fig. 7 shows the thus obtained van Deemter curves for two of the components appearing in the chromatograms of the phenone sample shown in Figs. 2 and 3. To emphasize the difference in band broadening one can expect when switching from a cF-mode to a cP-mode run delivering the same maximal pressure, the data of both modes have been plotted versus the F-value of the corresponding cF-run. For peak number 2 (Fig. 7a), the difference between the plate height curve obtained in the cF- and the cP-mode is relatively small. Nevertheless, a small, but significant difference between the first part and the second part of the van Deemter plot can be noted. In the first part (left of the H-minimum), the cP-mode plate height data are slightly smaller than those for the cF-mode, whereas the opposite holds in the second part (right of the H-minimum). In Fig. 7b, a similar observation can be made for the plate heights pertaining to peak number 9. Even more, the difference between the cF- and the cP-mode is significantly larger than for peak number 2 considered in Fig. 7a. This can be attributed to the fact that, for the presently considered gradient program, peak number 9 has witnessed a much larger difference in flow rate between the cF- and the cP-mode than the much earlier eluting peak number 2 (see the discussion of the difference between the two zoom-ins of Figs. 2 and 3). The difference in experienced flow rate can also be deduced from the real time chromatograms shown in Figs. 2a and 3a, showing that the cP-mode acceleration of peak number 2 is much smaller than that for peak number 9.

Given the dependency of the observed plate height differences, we found it instructive to calculate an average plate height, sum-

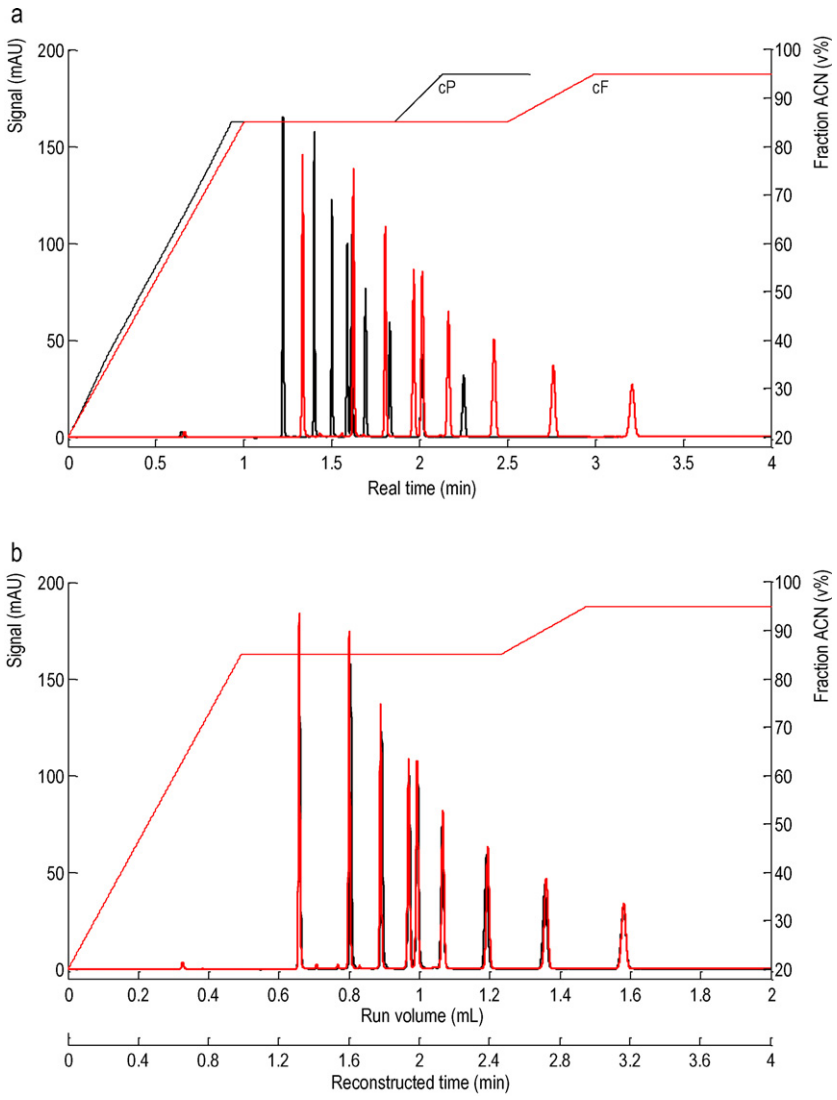

Fig. 6. Comparison of the chromatograms and the gradient program in cF- (red) and cP-mode (black) of the phenone mixture for a more complex gradient, as indicated on the Figure, measured on a 2.1 mm × 150 mm column and plotted versus the (a) real time and the (b) elution volume. (For interpretation of the references to color in text, the reader is referred to the web version of the article.)

ming the plate heights of the 9 individual peaks and calculating the average. The thus obtained plot is shown in Fig. 8a. As expected, the difference between the cF- and the cP-mode plate heights now lies somewhat in between the difference noted for peak number 2 in Fig. 7a (small difference in average flow rate between cF- and cP-mode) and that noted for peak number 9 in Fig. 7b (largest difference in average flow rate between cF- and cP-mode).

The general observation that can be made from Fig. 8a, i.e., that the cP-mode leads to smaller plate heights in the *B*-term dominated regime, whereas the opposite holds in the *C*-term, is in full agreement with the theoretical predictions made in part I, which in turn could be rationalized via the discussion of Fig. 5 of part I. In brief, the different behavior in the low and high flow rate range is due to the typical shape of the van Deemter curve. Because of this shape, the higher flow rates of the cP-mode lead to lower plate heights in the *B*-term dominated part of the curve, whereas the opposite occurs in the *C*-term dominated part of the curve. Quantifying the differences between the two modes observed in Fig. 8a, it can be said that, in the *B*-term dominated regime, the cP-mode leads to plate heights that are some 20–40% smaller than in the cF-mode (in fact the advantage of the cP-mode becomes larger with decreasing flow rate, in agreement with Eq. (27a) of part I). In the *C*-term dominated regime, the cP-mode leads to plate heights that are some 5–10% larger than in the cF-mode (here the disadvantage of the cP-mode in fact grows with increasing flow rate, in agreement with Eq. (27c) of part I).

Whereas the cP-mode plate height data in Fig. 8a have been plotted versus the flow rate F_F of the corresponding cF-mode run (to visualize the difference one can expect when running the cP- and the cF-mode with the same maximal pressure setting), it is obvious to expect that the band broadening in the cP-mode will rather be dominated by the average flow rate F_{av} than by the F_F-value (which only corresponds to the lowest flow rate experienced during the cP-run). With the tracked flow rate profile during the gradient, this average flow rate can readily be calculated. Subsequently re-plotting the cP-data of Fig. 8a versus F_{av}, the two plate height curves shift much closer to each other and nearly overlap. Certainly, the adopted determination of H_{av} (obtained by summing the *H*-values of the individual peaks and dividing the sum by the number of peaks) is most probably too simplistic to investigate the effect of the flow rate on the band broadening (not all peaks have witnessed the same average flow rate). Nevertheless, we believe the good agreement between the cF- and the cP-curve in Fig. 8b provides a good example of the fact that the velocity-dependency of

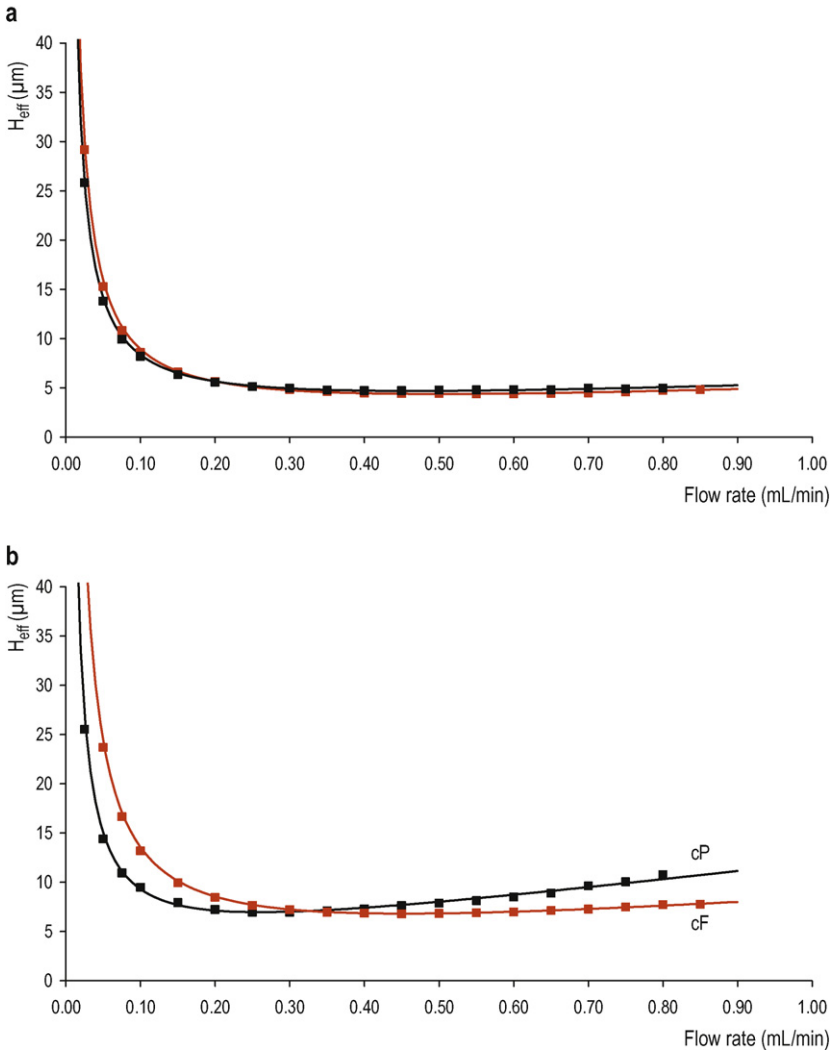

Fig. 7. Plot of the effective plate heights versus the (minimal) flow rate for the cF- (red) and the cP-mode (black) for (a) peak 2 and (b) peak 9 from the phenone mixture. The same conditions were used as in Fig. 2. The effective plate height is calculated with Eq. (8). (For interpretation of the references to color in text, the reader is referred to the web version of the article.)

the band broadening under gradient elution conditions can still be described by a fundamental reduced van Deemter curve (depending of course on the nature of the packing and the retention and diffusion history of the components). This is in line with the theoretical work presented in [18,23,24,36], and, as is shown here, even holds in the case of a variable flow rate.

3.4. Peak capacity measurements

Since gradient elution separations are more adequately described by the generated peak capacity than by the observed efficiency N (in part because of the additional difficulty that the $(1 + k_{loc,e})$-factor in Eq. (8) is not directly available), the peak capacity of each of the chromatograms used in the van Deemter analysis has been calculated. These calculations were made using the following expression:

$$n_p = 1 + \frac{V_{R,1} - V_{R,0}}{4\sigma_{v,1}} + \sum_{i=1}^{n-1} \frac{V_{R,i+1} - V_{R,i}}{4((\sigma_{v,i+1} + \sigma_{v,i})/2)} \quad (9)$$

As elaborated in part I, Eq. (9) is based on elution volumes instead of elution times because the time-based chromatogram does not reflect the actual separation resolution in the column when the flow rate varies with the time as is the case in the cP-mode. This implies that the correct peak capacity for the cP-mode should either be determined in the volume-based chromatogram or from the reconstructed time-based chromatogram. Applying Eq. (9) to the phenone sample ($n = 9$), the summation ran from $i = 1$ to $i = 8$, corresponding to the elution window between the first and the last eluting compound, whereas the first term of Eq. (9) represents the contribution to the peak capacity of the elution window between the dead time marker and the first component. Plotting the thus calculated peak capacity versus the real elution time of the last component, the fixed length kinetic plot curves shown in Fig. 9 are obtained [37]. These reflect the peak capacity that can be obtained on a column with given length for various values of total retention time (which is varied by varying the flow rate). Comparing the cF and cP elution mode, it can be noted that the cP-mode needs a shorter time to reach a given peak capacity than the cF-mode. Near the optimum of the curve, the difference between both modes is small.

As abundantly elaborated in Refs. [38–40], a fixed length kinetic plot as the one shown in Fig. 9 only provides a limited view on the performance limits of a given technique, because all data points (except the one corresponding to the highest velocity and the smallest retention time) relate to a sub-optimal pressure (in a fixed length format only the highest velocity data point can relate to the maximally available or allowable pressure). The fact that the

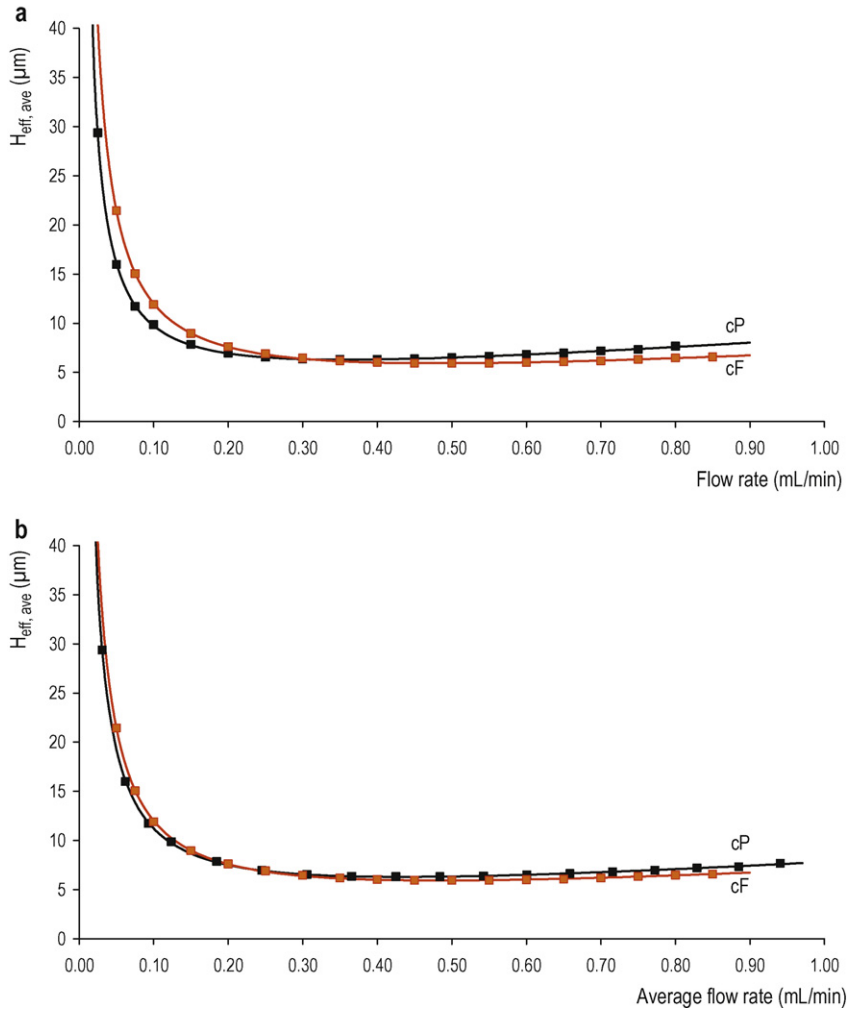

Fig. 8. Plot of the average effective plate height of the nine components of the phenone sample versus the (a) minimal flow rate and the (b) average flow rate for the cF- (red) and the cP-mode (black). The same conditions were used as in Fig. 2. The effective plate height is calculated with Eq. (8). (For interpretation of the references to color in text, the reader is referred to the web version of the article.)

represented data points relate to sub-optimal conditions for example explains why the cP-mode data points lie below the cF-mode data points over most part of the curves shown in Fig. 9. A much more correct view of the true kinetic performance potential (i.e., where each system operates at its kinetic optimum) is obtained in the free-length kinetic plot format, wherein each velocity data point of the original fixed length kinetic plot is transformed into the performance one can expect if the same velocity would be applied in a column that would just be long enough to achieve the given velocity when the pump operates at the maximal pressure. As shown in Ref. [41], this transformation can be readily done using a so-called column elongation parameter λ, which, in order to maximally account for the changes in viscosity caused by ultra-high pressure and viscous heating effects, should in its general form be written as [41]:

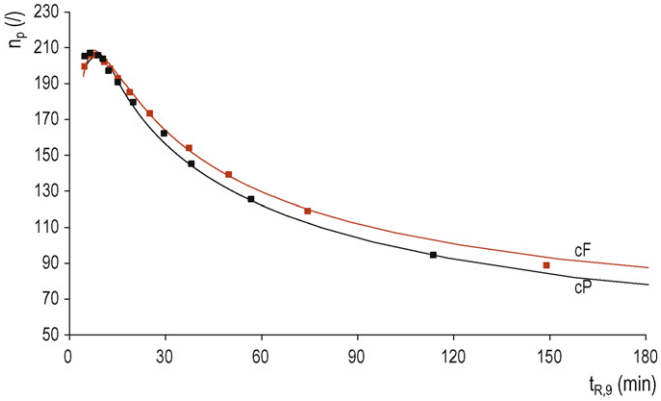

Fig. 9. Fixed length kinetic plot: peak capacity versus the analysis time for the phenone mixture (same gradient conditions as in Fig. 2).

$$\lambda = \lambda_{F_{max}} \cdot \frac{F_{max}}{F} \tag{10}$$

In Eq. (10), $\lambda_{F_{max}}$ is defined as the $\Delta P_{max}/\Delta P_{F_{max,exp}}$ value of the highest considered flow rate. In this ratio, ΔP_{max} is simply the maximally allowable instrument or column operating pressure drop, while ΔP_{exp} is the maximal value of the column pressure drop measured during the cF-mode experiment performed at the highest flow rate or the actually imposed column pressure drop during the corresponding cP-experiment.

The value of λ (which is different for each different velocity point in the recorded fixed length kinetic plot) can then be subsequently used to transform the experimentally measured peak capacity and analysis time values obtained on the fixed length column into the corresponding values of the free length kinetic plot curve. Since in this curve the data points are assumed to be obtained in a col-

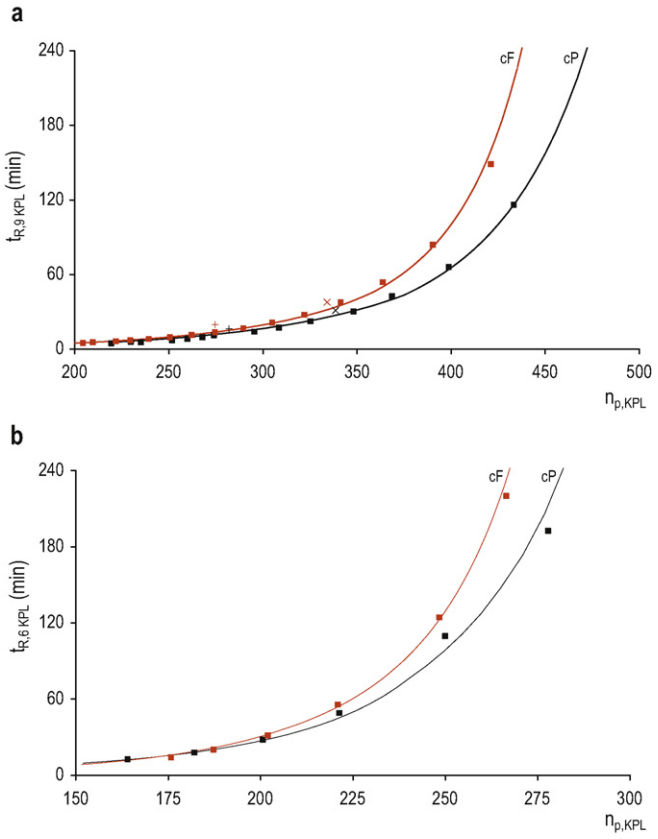

Fig. 10. Kinetic plot limit curves for 1200 bar comparing the cF- (red) and cP-mode (black) for the (a) phenone mixture (same gradient conditions as in Fig. 2) and the (b) alkylbenzene mixture (same gradient conditions as in Fig. 5). For the phenone mixture, the experimentally measured peak capacity on a 250 mm (+) and a 350 mm (×) coupled column have been added as well (P_{max} = 1052 bar, F_{min} = 0.400 mL/min and P_{max} = 1117 bar, F_{min} = 0.275 mL/min, respectively). (For interpretation of the references to color in text, the reader is referred to the web version of the article.)

umn operated at the maximal pressure, they represent the kinetic performance limit (KPL) of the investigated technique

$$t_{R,KPL} = \lambda t_{R,exp} \quad (11)$$

$$n_{p,KPL} = 1 + \sqrt{\lambda}(n_{p,exp} - 1) \quad (12)$$

To properly account for the effect of the operating pressure on k_{eff} (see Fig. 4), the right hand side of Eqs. (11) and (12) should be multiplied with a factor $(1 + k_{eff,F_{max}})/(1 + k_{eff})$, as discussed in the SM of [41].

Applying this transformation to the peak capacity and retention time data (last eluting compound) shown in Fig. 9, the free length KP-curve (KPL-curve) shown in Fig. 10a is obtained for a pressure limit of 1200 bar. A similar transformation was done for the separations carried out with the alkylbenzene sample and the water–methanol gradient (see Fig. 5). The corresponding KPL-curve is shown in Fig. 10b.

The two additional data point couples added to Fig. 10a (cf. the straight and tilted crosses) represent the actually measured peak capacity and analysis time at the pressure limit on two longer columns than the one on which the KPL-transformation is based (resp. 250 mm and 350 mm versus 150 mm). This was done to experimentally verify the validity of the KPL-transformation. As can be noted, the agreement between the KPL-prediction and the experimental verification is close, but not perfect. A small offset in the peak capacity can be noted when comparing the measurements made on the coupled column systems with those made on the single 150 mm column. This is because the 150 mm column efficiency

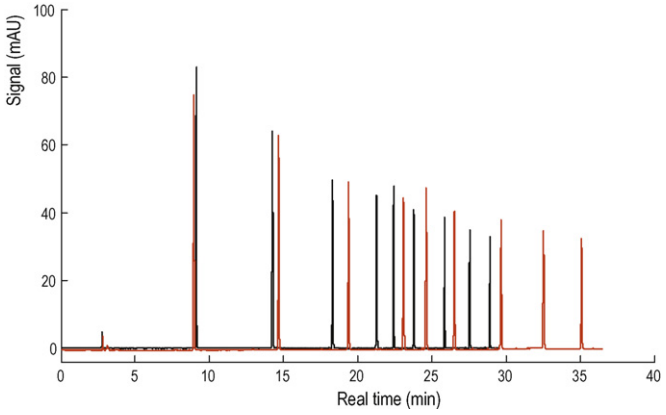

Fig. 11. Comparison of the chromatograms and the gradient program in cF- (red) and cP-mode (black) of the phenone mixture on a coupled 2.1 mm × 350 mm column (P_{max} = 1117 bar, F_{min} = 0.275 mL/min). The same gradient conditions as in Fig. 2 were used. (For interpretation of the references to color in text, the reader is referred to the web version of the article.)

is relatively higher (see efficiency values cited in Section 2.1) compared to the two 100 mm columns that were used to construct the 250 and 350 mm coupled columns. If the data-points would be corrected for this difference in efficiency, they would coincide with the predicted KPL-curve for both the constant flow and constant pressure measurements.

The KPL-curves established on the basis of the 150 mm column (full symbols, solid fitting line) show that the kinetic performance limit of the cP-mode is superior to that of the cF-mode since the kinetic performance limit in the cP-mode lies consistently below the cF-mode. The improvement is especially significant in the range of large peak capacities and long run times. In the range of short elution times, the gain of the cP-mode becomes insignificant, as the cF- and the cP-mode curves clearly converge. The shape and mutual position of the curves is in full agreement with the theoretical predictions in part I, where it was indeed shown that the cP-mode and cF-mode curves can be expected to converge in the *C*-term dominated range (range of short elution times) because the gain in analysis time is in this range counterbalanced by an equivalent loss in efficiency.

Considering high efficiency separations on long columns, where even at the maximal pressure only flow rates below or around the optimal flow rate can be achieved, the cP-mode clearly performs better. It is illustrated by the example obtained on the 350 mm long coupled column (tilted crosses in Fig. 10a), where the average flow rate was at 0.275 mL/min and 0.332 mL/min for the cF- and cP-mode, respectively, i.e., slightly below the optimal flow rate (≅0.4 mL/min) corresponding to the minimum of the van Deemter plot in Fig. 8b. As can be noted from the corresponding chromatogram in real time units (Fig. 11), switching to the cP-mode allows to finish the run in 29 instead of in 35 min, while also a larger peak capacity (based on the chromatogram plotted in volumetric or reconstructed time units) is obtained (going from 334 in the cF-mode to 339 in the cP-mode). Coupling even more columns, so as to shift even more to the right on the KPL-curve, the further divergence of the cF- and the cP-mode curves suggest that the gain in both analysis time and peak capacity can be expected to be even larger. However, since these performances are anyhow related to flow rates that are situated in the *B*-term dominated range, this gain is not relevant for most practical applications since a separation that is run in the *B*-term regime can always be replaced by one with larger particles than the presently considered sub 2 μm-particles.

A fully similar trend is observed for the KPL-data collected with the alkylbenzene sample and the water–methanol gradient (Fig. 10b). Compared to the water–acetonitrile gradient, lower peak

capacities are obtained due to the intrinsic fluidic properties of methanol compared to acetonitrile (viscosity and diffusion coefficient), but also due to the lower gradient slope in the case of the water–acetonitrile gradient.

4. Conclusions

The possibility to operate an ultra-high pressure pump at a constant pressure during gradient elution with a volume-based gradient program has been demonstrated under various conditions. Identical volume-based gradient programs could be run in both modes, i.e. in the constant flow rate mode as well as in the constant pressure mode, resulting in identical separation selectivities and relative peak elution patterns, which is in full agreement with the theory of part I.

The constant pressure mode offers the distinct advantage that the run time can be shortened with respect to the constant flow rate mode, while maintaining the same selectivity. The realized gains were in good agreement with the gains predicted in part I on the basis of the intrinsic relation between the viscosity and the composition of the water/organic mixtures and assuming an isothermal operation. For gradients running between 5 and 95% and operated in the ultra-high pressure range, some 17% reduction in analysis time has been demonstrated, in agreement with the theoretical expectations. Gains of over 25% were obtained for a segmented gradient with flat segments in the region with lower solvent viscosity. In practice, these gain values should be increased by some 5–10%, as this is the pressure safety margin one usually needs to leave if running a cF-operation. Taking this into account, the realized time gains are rather in the 25% range (linear gradient), and may run up to 35% (segmented gradients with flat segments in the region with lower solvent viscosity).

Comparing a cP- and an cF-mode seperation conducted at the same maximal pressure (which in the cF-mode is only reached during a brief instant), the cP-mode leads to plate heights that are some 20–40% smaller than in the cF-mode in the *B*-term dominated regime, while they are some 5–10% larger in the *C*-term dominated regime. This difference is caused by the fact that both modes inevitably subject the analytes to a different velocity history. Compensating for this different velocity history by plotting the Van Deemter curve of the cP-mode plate height data as a function of the average flow rate, the difference between modes nearly completely vanishes, as the obtained cP-curve agrees closely with the plate height curve obtained in the cF-mode. This confirms the theoretical expectation [23,25,36] that, even under gradient elution conditions and under conditions of a variable flow rate, the band broadening in a chromatographic column is dominated by a universal reduced plate height curve (depending of course on the nature of the packing and the retention and diffusion history of the components).

Combining efficiency and selectivity into a kinetic plot of gradient peak capacity versus time, it is found for the two considered combinations of organic modifier and sample type that the kinetic performance limit of the cP-mode is consistently better than that of the cF-mode, although the gain of the cP-mode becomes insignificant for separations with a flow rate in the *C*-term controlled range. As such, the obtained curves are in full agreement with the theoretical predictions in part I. For lower flow rates, the gain that can be obtained by switching to the cP-mode can be substantial. Considering a separation with sub 2-μm particles on a 350 mm long coupled column, operated at a (maximal) pressure of about 1200 bar, switching to the cP-mode allows to finish the run in 29 instead of in 35 min, while also a larger peak capacity (based on the chromatogram plotted in volumetric or reconstructed time units) is obtained (going from 334 in the cF-mode to 339 in the cP-mode).

List of symbols

A	column cross section [m^2]
cF	constant flow rate operation
cP	constant pressure operation
F	mobile phase flow rate [m^3/s]
F_F	flow rate during a cF-mode run [m^3/s]
F_{max}	maximum experimental flow rate [m^3/s]
F_{av}	volume average flow rate in the cP-mode run [m^3/s]
H	(local) plate height [m]
H_{av}	plate height averaged for different components [m]
H_{eff}	column length averaged effective plate height [m]
k	retention coefficient
k_{loc}	local retention coefficient
K_{V_0}	u_0-based column permeability [m^2]
KPL	kinetic performance limit
L	column length [m]
N	theoretical plate count
n_p	peak capacity
ΔP_{col}	column pressure drop [Pa]
ΔP_{max}	maximum allowed column or instrument pressure drop [Pa]
S	linear solvent strength parameter
t	time [s]
t_G	gradient time [s]
t_R	retention time [s]
t_V	volume-based reconstructed time, see Eq. (1) [s]
t_0	column dead time [s]
V	volume [m^3]
V_G	gradient volume [m^3]
V_R	retention volume or the volume pumped through the column at the instant at which the peak centroid elutes from the column [m^3]
V_0	column dead volume, defined as $A{\cdot}\varepsilon_T{\cdot}L$ [m^3]
β	gradient steepness, see Eq. (2)
ε_T	total porosity
ϕ	fraction of organic modifier in mobile phase
ϕ_e	fraction of organic modifier in mobile phase at the end of the gradient
ϕ_0	fraction of organic modifier in mobile phase at the start of the gradient
η	viscosity [Pa s]
$\bar{\eta}$	average column viscosity [Pa s]
λ	column length rescaling factor, defined in Eq. (10)
σ_V	volumetric standard deviation [m^3]

Acknowledgements

The Department of Chemical Engineering of the VUB gratefully acknowledges the loan of a modified Agilent 1290 system from Agilent Waldbronn GmbH and a University Relation grant from Agilent Technologies, University Relations and External Research. M.V. and K.B. gratefully acknowledge research grants from the Research Foundation – Flanders (FWO Vlaanderen).

References

[1] L.R. Snyder, J.J. Kirkland, Introduction to Modern Liquid Chromatography, second edition, Wiley, New York, USA, 1979.
[2] W. Wiedemann, H. Engelhardt, I. Halász, J. Chromatogr. 91 (1974) 141.
[3] H. Engelhardt, Z. Anal. Chem. 277 (1975) 267.
[4] B.J. McCoy, J. Chromatogr. Sci. 291 (1984) 339.
[5] J. Plockova, J. Chmelik, J. Chromatogr. A 918 (2001) 361.
[6] J.H. Block, J.W. Ayres, D.R. Henry, H.L. Levine, J. Chromatogr. 193 (1980) 111.
[7] F. Houdiere, P.W.J. Fowler, N.M. Djordjevic, Anal. Chem. 69 (1997) 2589.
[8] S. El Deeb, U. Schepers, H. Wätzig, J. Sep. Sci. 29 (2006) 1571.
[9] V. Lesins, E. Ruckenstein, J. Chromatogr. 467 (1989) 1.

[10] P. Nikitas, A. Pappa-Louisi, K. Papachristos, C. Zisi, Anal. Chem. 80 (2008) 5508.
[11] A. Pappa-Louisi, P. Nikitas, A. Zitrou, Anal. Chim. Acta 573–574 (2006) 305.
[12] K. Papachristos, P. Nikitas, J. Chromatogr. A 1216 (2009) 2601.
[13] H.W. Habgood, W.E. Harris, Programmed Temperature Gas Chromatography, J. Wiley and Sons, N.Y, 1966.
[14] C.F. Poole, S.K. Poole, Chromatogr. Today, Elsevier, Amsterdam, 1991.
[15] M.H. Chen, C. Horváth, J. Chromatogr. A 788 (1997) 51.
[16] L.R. Snyder, J. Chromatogr. 13 (1964) 415.
[17] L.R. Snyder, J. Chromatogr. Sci. 8 (1970) 692.
[18] L.R. Snyder, J.W. Dolan, J.R. Gant, J. Chromatogr. A 165 (1979) 3.
[19] P. Jandera, J. Churacek, J. Chromatogr. 91 (1974) 223.
[20] P. Jandera, J. Chromatogr. A 1126 (2006) 195.
[21] P.J. Schoenmakers, H.A.H. Billiet, R. Tijssen, L. de Galan, J. Chromatogr. 149 (1978) 519.
[22] M. Martin, J. Liq. Chromatogr. 11 (1988) 1809.
[23] U.D. Neue, J. Chromatogr. A 1079 (2005) 153.
[24] F. Gritti, G. Guiochon, J. Chromatogr. A 1212 (2008) 35.
[25] U.D. Neue, H.J. Kuss, J. Chromatogr. A 1217 (2010) 3794.
[26] L.R. Snyder, J.W. Dolan, High Performance Gradient Elution. The Practical Application of the Linear-Solvent-Strength Model, Wiley–Interscience, Hoboken, NJ, USA, 2007.
[27] J. Billen, K. Broeckhoven, A. Liekens, K. Choikhet, G. Rozing, G. Desmet, J. Chromatogr. A 1210 (2008) 30.
[28] J.W. Thompson, T.J. Kaiser, J.W. Jorgenson, J. Chromatogr. A 1134 (2006) 201.
[29] J. Li, P.W. Carr, Anal. Chem. 69 (1997) 2530.
[30] U.D. Neue, J. Chromatogr. A 1184 (2008) 107.
[31] B. Drake, Akriv. Kemi 8 (1955) 1.
[32] E.C. Freiling, J. Am. Chem. Soc. 77 (1955) 2067.
[33] E.C. Freiling, J. Phys. Chem. 61 (1957) 543.
[34] A. de Villiers, H. Lauer, R. Szucs, J. Chromatogr. A 1113 (2006) 85.
[35] D. Cabooter, F. Lestremau, A. de Villiers, K. Broeckhoven, F. Lynen, P. Sandra, G. Desmet, J. Chromatogr. A 1216 (2009) 3895.
[36] H. Poppe, J. Paanakker, M. Bronckhorst, J. Chromatogr. 204 (1981) 77.
[37] G. Desmet, D. Clicq, P. Gzil, Anal. Chem. 77 (2005) 4058.
[38] G. Desmet, D. Clicq, D.T.T. NGuyen, D. Guillarme, S. Rudaz, J.-L. Veuthey, N. Vervoort, G. Torok, D. Cabooter, P. Gzil, Anal. Chem. 78 (2006) 2150.
[39] S. Eeltink, G. Desmet, G. Vivo-Truyols, G. Rozing, P.J. Schoenmakers, W.Th. Kok, J. Chromatogr. A 1104 (2006) 256.
[40] G. Desmet, D. Cabooter, LC–GC Europe 22 (2009) 70.
[41] K. Broeckhoven, D. Cabooter, F. Lynen, P. Sandra, G. Desmet, J. Chromatogr. A 1217 (2010) 2787.